

1,2\*Sheng He,  
3,4,5\*Wenxin Ma,  
3,4,5Jun Pan

## Exploring Medium and Low-Temperature Convective Geothermal Resources Through Controlled Source Audio Magnetotelluric Method



**Abstract:** Medium and low-temperature convective geothermal resources are a crucial component of China's geothermal wealth, primarily concentrated in the eastern coastal regions. To maximize the utilization of these resources, geophysical surveys are essential, with controlled source audio magnetotelluric (CSAMT) being a prominent and effective method employed in geothermal resource assessments. This study focuses on applying CSAMT to survey specific geothermal sites, including the Xiu Yan Gou Tang Hot Spring, Fengcheng Gou Tang Hot Spring, and Hai Cheng Xi Huang di Geothermal Field. The results obtained through this method provide detailed insights into the distribution of both deep and shallow thermal storage spaces within these fields, shedding light on the intricate thermal circulation systems associated with them. These findings serve as a reliable foundation for planning and executing further geothermal resource development projects. CSAMT emerges as a comprehensive tool for understanding the nuances of medium and low-temperature convective geothermal resources.

**Keywords:** low and medium temperature convective geothermal; fracture structure; deep thermal reservoir; shallow thermal reservoir; CSAMT

### I. INTRODUCTION

Geothermal energy is hailed as a premium renewable energy source, characterized by its low carbon emissions and abundant reserves, making it a pivotal resource in the context of growing environmental concerns and resource scarcity [1]. To harness geothermal energy more effectively, conducting precise site surveys to comprehend the specific distribution patterns of geothermal resources is imperative. Geomagnetic bathymetry stands out as a crucial method in the realm of geothermal energy exploration, owing to its ease of operation and provision of reliable results. Therefore, there is a pressing need to advance the technical research associated with this method to optimize its application [2].

Geomagnetic bathymetry relies on the analysis of subsurface resistivity disparities to unveil subsurface thermal storage. In practical applications, the key reference point is the measured resistivity data. Based on these data, a reasonably accurate determination of the spatial distribution of geological formations and the location of thermal reservoirs is made [3]. Field surveys are typically conducted using robust and dependable multifunctional electromagnetic instruments, supported by the MtSoft2D software, which aids in the efficient processing and analysis of the collected data.

The controlled source audio magnetotelluric (CSAMT) method is a commonly used method with outstanding application in detecting low resistance anomalies [4]. It has multiple advantages such as large exploration depth, ability to adapt to the field environment, high resolution, ease of operation and economic efficiency, and is therefore widely used in the field of geothermal resource exploration and plays an important role in the current geothermal exploration [5].

The CSAMT method is a new method derived from the prototype of the geomagnetic method (MT method) with theoretical and technical upgrades, and is a more typical electromagnetic exploration method in the frequency

<sup>1</sup> Xining Natural Resources Comprehensive Survey Center, China Geological Survey, Xining 810021, China;

<sup>2</sup> School of Water Resources and Environmental Engineering, East China University of Technology, Nanchang 330013, China;

<sup>3</sup> Key Laboratory of Environmental Geology of Qinghai Province, Xining 810008, China;

<sup>4</sup> Qinghai 906 Engineering Survey and Design Institute, Xining 810007, China;

<sup>5</sup> Qinghai Bureau of Environmental Geology Exploration, Xining 810008, China;

\*First author: Sheng He, Senior engineer, His research interests include application and Research of Electromagnetic Detection Technology, etc.; [hesheng1399@163.com](mailto:hesheng1399@163.com) \*Corresponding author: Wenxin Ma, engineer, His research interests are geothermal geophysical prospecting; [13327636767@163.com](mailto:13327636767@163.com)

domain at this stage [6]. In the application of this method, the orthogonal electric and magnetic field components are observed following the MT method, calculations are organized based on the measured data, the Canea apparent resistivity is determined, and the characteristics of the subsurface electrical distribution are explored based on the data.

Depending on the number of field sources and the observed field components, the CSAMT method can be subdivided to obtain three forms: tensor, vector and scalar. The tensor and vector methods are not yet available as a mature method due to the late start of the technology, the limited level of data acquisition, and the poor feasibility of supporting instruments.

The CSAMT method has the following application advantages: ① Overcomes the problem of weak natural field signals in the conventional MT method and has excellent immunity to interference throughout the application. (ii) It has a stronger exploration capability compared to DC and transient electromagnetic methods, and can usually be used for deep exploration tasks. ③ High lateral resolution enables fast and accurate detection of faults; in addition, it has a certain degree of vertical resolution, which makes reasonable stratification of strata more convenient. ④ The dual function of bathymetry and profile study helps to improve exploration efficiency. ⑤ The stability of the alternating electromagnetic field is good, and it can penetrate high resistance layers. Because of this characteristic, the CSAMT method is widely used in geological surveys and geothermal resource exploration, and the geological information measured is accurate and reliable.

## II. PRINCIPLE OF CSAMT OPERATION

In the CSAMT method of exploration, the field generated at ground level by a point source or magnetic dipole in a homogeneous half space is usually studied. This is because the tectonic electromagnetic method of exploration is observed at ground level. According to field theory, electromagnetic waves generated by dipole antennas actually radiate in all directions [7]. Depending on the propagation path of the waves, they can be divided into celestial, terrestrial (waves) and stratigraphic (waves) waves, as shown in Figure 1. Because of the difference in wave range between ground and stratigraphic waves, ground waves propagating along the surface and stratigraphic waves propagating directly in the earth will form an approximately horizontal wavefront near the ground at a certain moment  $t$ , producing waves that propagate almost vertically downwards, i.e., approximately horizontally polarized plane waves (waves), as shown in Figure 1(b). The wave, wave and wave interact with the subsurface geological body during propagation and reflect the result of the interaction to the surface observation point.

According to the skin effect of the propagation of AC electromagnetic fields in the medium, electromagnetic fields of different frequencies have different penetration depths. At high frequencies, the electromagnetic fields are distributed at shallow depths; at low frequencies, they are distributed at deeper depths. Therefore, by varying the emission frequency, it is possible to study the geological situation at different depths in the subsurface [8]. In electromagnetic theory, the depth required for the electromagnetic field ( $E, H$ ) to attenuate to  $1/e$  times its initial value as it propagates through the earth is defined as the penetration depth or skinning depth. It is calculated as shown in Equation 1:

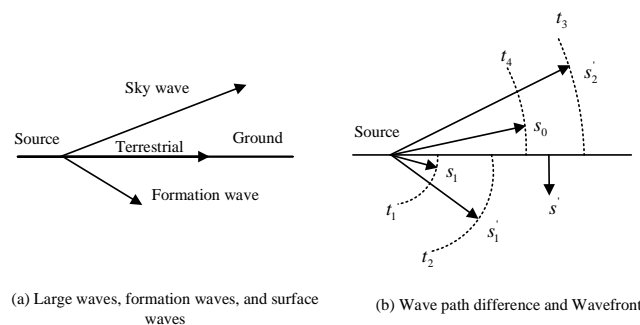


Figure 1 Electromagnetic wave propagation pathways

$$\delta = \sqrt{\frac{\rho}{\pi f \mu}} \quad (1)$$

Where  $\delta$  is the skinning depth;  $f$  is the frequency in Hz;  $\rho$  is the resistivity in  $\Omega \cdot m$ ;  $\mu$  is the permeability of the medium. As can be seen from equation (1), the skinning depth will vary with resistivity and frequency. In general, data at higher frequencies in the frequency domain EM method reflect shallow electrical information, and data at lower frequencies reflect deeper electrical information. Therefore, by observing the electric and magnetic field information over a wide frequency band and calculating the apparent resistivity and phase from it, the electrical distribution characteristics of the subsurface media can be inferred, and thus the geological structure of the subsurface media can be studied. In the CSAMT method of exploration, the frequency of the electromagnetic fields can be selected according to the specific situation.  $H_y, E_x$  and their phase  $\phi H_y, \phi E_x$  can be obtained in real time in the field, and 1D inversion and 2D resistivity imaging can be performed, and 2D forward and inverse results can be obtained after indoor data processing.

### III. DATA QUALITY ASSURANCE MEASURES AND DATA RELIABILITY ANALYSIS

In the field data acquisition process, we used the multifunctional electro-magnetic detection system GD-32 II, a fourth generation multi-channel receiver for electro- and electromagnetic detection of controlled and natural field sources from Zon ge Engineering, USA [10]. In selecting the electric field sources, emission points and transceiver distances within the work area, we carefully selected the most suitable emission source locations for this survey area in order to provide as high a current as possible while meeting the exploration requirements, improve the signal-to-noise ratio, etc., and lay a good foundation for the quality of the field data.

An equatorial dipole device was used as the deployment method and the scalar measurement method of the CSAMT method was used. The electrode MN for the electric field component  $E_x$  is arranged horizontally, parallel to the supply pole AB, while the horizontal magnetic field  $H_y$  is laid perpendicular to the field source [11]. the distance between AB and MN (transceiver distance  $r$ ) is a minimum of 8 km. The distance between the magnetic rods and the preamplifier is greater than 5 m. To eliminate human interference, the two rods need to be buried underground to maintain stability [12]. We used a compass meter for orientation so that the two magnetic rods,  $H_x$  and  $H_y$ , were perpendicular to each other and horizontal, controlling the error to within 2 degrees. All staff were placed at least 5m away from the rods and the rods were placed as far away from houses, cables and large trees as possible. During construction, we used 50Hz trapped waves to place the line arrangement and actual measurements as far away from sources of interference as possible.

A certain amount of quality data checks were carried out in the measurement area. Two repeat observations were made at different times using the same parameters and the consistency of the resulting data was compared to analyze the reliability of the data [13]. Table 1 demonstrates a comparison of the data from two actual test experiments at a checkpoint in the survey area. As can be seen from Table 1, the root mean square error was controlled to be below 3.47%, indicating that the data quality was well controlled and met the design and specification requirements.

Table 1 Comparison of measured data at an inspection site in the field

Frequency	Original measurement (Kania apparent resistivity)	Retest (Kania apparent resistivity)	Difference	Mean squared error/%
5766	2517.5	2522.4	-4.8	0.000005
8193	13	13.114	-1.112	0.007858
2883	2773	2774.8	-2.6	0.000002
4097	1861.9	1863.59	-1.77	0.000002
1442	2034.0	2037.14	-3.22	0.000004
2049	3784.6	3881.4	-97.7	0.000652
722	2842.5	2845.4	-2.8	0.000002

1025	1926.4	1929.9	-3.4	0.000004
361	5460.0	5455.4	4.7	0.000002
513	3929.7	3934.2	-4.4	0.000002
181	8343.2	8355.8	-12.5	0.000003
257	6899.5	6999.4	-99.8	0.000208
91	11512	11617	-104	0.000083
129	10184	10190	-5	0.000000
46	14980	15152	-171	0.000131
65	14635	14218	418	0.000837
22.6	23199	22990	210	0.000083
33	21141	20180	962	0.002165
11.4	40644	40601	44	0.000002
17	33156	33352	-195	0.000036
5.64	76359	76600	-240	0.000011
9	61375	60100	386	0.000041
2.82	168041	167321	721	0.000019
5	111201	110901	301	0.000008
1.42	229091	190003	39089	0.034797
3	291061	300002	-8940	0.000916
2	624331	602222	22110	0.001301
0.6	589994	584322	5673	0.000094
0.26	789322	782134	7189	0.000085
0.126	578652	577751	902	0.000003

#### IV. SURVEY METHODS AND SURVEY AREAS

##### A. Survey area

In the field data acquisition process, the GDP-32II multifunctional Electrophotometer manufactured by Zon ge, USA was used. The CSAMT was measured scalarly using an equatorial dipole device with a supply pole distance AB of 1,000 m, a transceiver distance  $r$  greater than or equal to 5,000 m, a measurement electrode distance MN of 50 m and a measurement point distance of 50 m. Data inversion was carried out using a one-dimensional circular slip model inversion interpretation method, using inversion resistivity sections for geological interpretation [14].

The elevation of the study work area is about 2,800~3,400m, and the area generally shows a high east to low west and high south to low north. Permian metamorphic rocks and Quaternary strata are widely distributed, with the former including slate, tuff and dolomite, and the latter including sand, gravel and pebbles.

There is also a larger range of magmatic rocks in a variety of forms, including Mesozoic and plagioclase granites.

##### B. Data acquisition and processing of controlled souce audio magnetotelluric (CSAMT) bathymetry

In the field data acquisition, we chose the multi-functional electro-meter V8 to collect the audio geodetic electromagnetic data. The distance of the bathymetry point is uniformly controlled at 20~40 meters, and the unpolarized electrode is used as the receiving electrode and the tension observation method is adopted. In order to make full use of the application value of the data, MTsoft2D2.3 software was introduced, which has powerful data processing capabilities and highly reliable results [15]. The software was developed using a modular approach with a core composition consisting of four modules: data management, data pre-processing, data inversion and results display, providing data processing and display functions through a joint application.

After all the basic preparations were in place, we first transferred the data collected in the field to the computer and started the software for editing operations. The basic aim of this stage was to remove obvious interference points and identify data where static effects were present, and to spatially filter this data [16]. Based on the results of the aforementioned processing, a frequency-apparent resistivity contour map is generated and a further 2D inversion operation is performed to generate the corresponding cross-sectional map for the analysis of the detection area. The

geomagnetic method takes full account of the differences in resistivity parameters, and the differences in this metric are used to delineate stratigraphic boundaries and geological formations and to determine the distribution of thermal reservoirs [17]. By collecting data and synthesizing geological information, we are able to make more systematic inferences about the distribution of geothermal resources, thus deepening our understanding of subsurface thermal resources.

## V. EXPLORATION EXAMPLES

### A. Xiu Yan Gou Tang Hot Spring

The Gou Tang hot spring is located in the Taikoo Basin vectorial axis, and the area of the hot spring is mainly composed of schist, metagranite and crystalline tuff of the Gai County Formation of the Liao he Group [18]. On the outer flanks of the hot spring area, gneisses, dacites and metagranites of the Da Shi Qiao Formation of the Liao he Group are exposed in order from the inside to the outside; gneisses, gneisses and hornblende of the Gao jia yu Formation of the Liao he Group; and metagranites, metavolcanic rocks, gneisses and dacites of the Lira yu Formation of the Liao he Group. In the western part of the hot spring area, there are outcrops of Huang Ling Zi amphibolite and diorite granite rocks [19]. The area consists mainly of fracture formations, the main ones being the north-east-trending Da Ying zi-Cao he Kou Deep Fault, about 130 km long and between 1 and 3 km wide, and the north-west-trending Xia mu Cheng-Sui Yan Fault, about 150 km in length.

The hot springs have an outcrop elevation of 174 rice and are of the convective geothermal type. The average water temperature of the hot springs ranges from 45 to 51 degrees Celsius and the volume of water produced exceeds 2,000 cubic rice per day.

The Quaternary in the area is very thin and has relatively little influence on the measured resistivity; the Liao He Group is a highly resistive formation and the resistivity should be greater than 5 000  $\Omega$ -m. If relatively low resistance occurs at a certain depth in the section through which the profile passes, a resistivity anomaly can be identified.

Figure 2 shows a composite profile from an CSAMT survey at Gou yu Hot Springs, where the hot springs are exposed near  $x = 750\text{m}$ . As can be seen from Figure 2, the overall resistivity (averaging greater than  $n \times 100 \Omega \cdot m$ ) within the profile is high and it is inferred that the entire profile should be within the Liao he Group within the bathymetric range; further stratification of the Liao he Group cannot be carried out as the resistivity of the rocks is similar in all sections of the group within the area. A high resistance layer appears at the surface of the profile, below which is a relatively low resistance layer, approximately 100m thick, which becomes deeper and shallower from the beginning to the end of the profile. At  $x = 750\text{m}$  the low resistance layer becomes less deep and is the outcrop point of the hot spring. Based on the measured resistivity, it is inferred that the shallow low-resistance layer is generated by the shallow thermal reservoir from the start of the profile to  $x = 1,000\text{m}$ , while from  $x = 1,000\text{m}$  to the end of the profile, the shallow low-resistance layer is generated by the increased mud content of the formation.

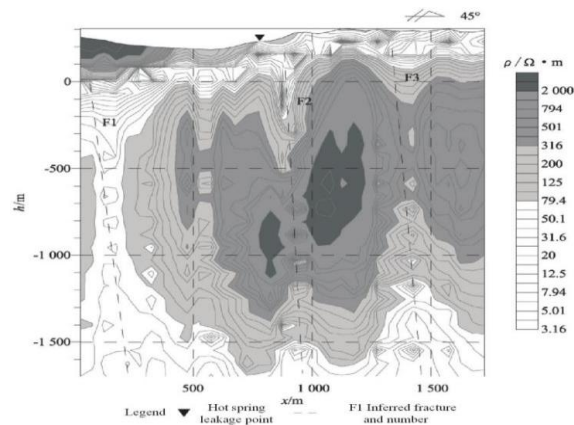


Figure 2 Gou yu Hot Spring CSAMT survey composite section

At distances of  $x = 150\text{m}$ ,  $950\text{m}$  and near  $1400\text{m}$ , distinct longitudinal low resistance zones occur. These longitudinal low resistance zones are presumed to have been generated by fracture formations, labelled F1, F2 and F3 respectively, where the F2 fracture is thought to be a hot water upwelling channel, while the fractures on either side of F1 and F3 are atmospheric precipitation recharge channels.

The profile demonstrates the resistivity anomaly characteristic of a typical convective geothermal field. A low-resistance thermal reservoir overlain by a high-resistance cover is evident in the shallow part of the profile, and hot springs occur right at the thinnest part of the high-resistance cover. The relatively low resistance areas in the deeper part of the profile represent the deeper thermal reservoirs [20]. The fracture formations create heat rise channels that connect to the shallow thermal reservoirs, effectively recharging the shallow heat sources. The fractures on either side are considered to be atmospheric water descent channels, based on inferences from the topography and geomorphology.

This example clearly demonstrates how the results of CSAMT can graphically describe the distribution of thermal storage space and the associated thermal circulation system in this type of geothermal field.

### B. Feng Cheng Gou Tang Hot Spring

Based on the results of the CSAMT survey of Gou yu Hot Springs, a composite profile is shown in Figure 3. As can be seen from Figure 3, the resistivity is high throughout the section. At  $x = 500\text{-}700\text{m}$ , the shallow part shows a low resistance zone, which can be inferred to be generated by the shallow thermal reservoir. Ignoring the relative influence of the shallow thermal reservoir on the overall resistivity, the shallow low-resistance layer is very thin, indicating that the Quaternary strata are very thin and have little influence on the measured resistivity; while below the Quaternary should be a rock body, which should have a resistivity greater than  $5,000 \Omega\cdot\text{m}$ .

Between  $x = 200\text{-}700\text{m}$  of the profile, a longitudinal zone of relative low resistance appears, and this zone of low resistance should be generated by the F1 and F2 fractures and their influence zones. And below  $h = -1400\text{m}$ , the relative low resistance occurs between  $x = 400\text{-}700\text{m}$ , which can be identified as the deep thermal reservoir, while the F1 and F2 fracture structure should be the hot water uplift channel.

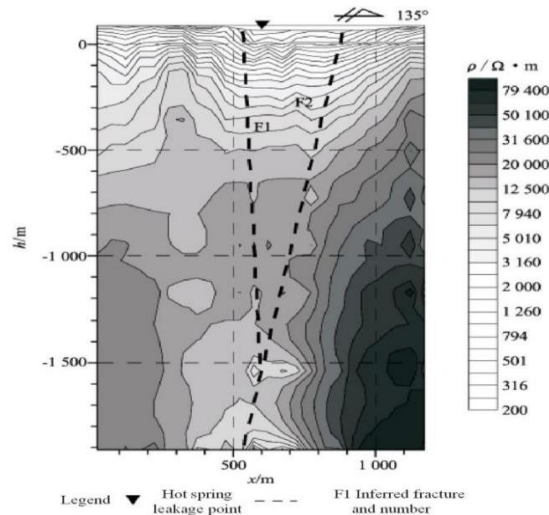


Figure 3 Gou yu Hot Spring CSAMT survey composite section

This example depicts another type of spatial distribution of medium to low temperature thermal storage, where deep subsurface hot water is channeled through fractures directly to the surface to form a thermal reservoir. Although the thermal reservoir is very thin, the results of the CSAMT can reveal the fracture spreading within the profile, the shallow and deep thermal reservoir storage space and the deep hot water upward channel.

C. Hai Cheng Xia di Geothermal Field

According to the actual data of the geothermal field area, the Quaternary is the overburden of the surface, and the borehole reveals that the lower part of the Quaternary is a granite body, while the Neoproterozoic still remains in local sections. The Quaternary consists mainly of clay, sub-clay, sand and gravel layers, while the Neogene consists mainly of sandstone and sand conglomerate. Granite ( $\gamma$ ) is a Middle Jurassic intruded granite body interspersed with amphibolite veins [21]. Statistical results show that the resistivity of the Quaternary is about 10-20  $\Omega$ -m with an average thickness of 100 m; the resistivity of the Neogene is about 30  $\Omega$ -m with a thickness between 20-70 m; and the resistivity of the granite is greater than 2,000  $\Omega$ -m.

Actual information indicates that underground hot water is mainly found in fractures and fissures within the granite body. Due to the relatively thick Quaternary overburden, the tectonic spreading and extension of the subsurface rock masses cannot be determined at the surface. Physical soundings such as transient electromagnetic sounding, direct current resistivity sounding and magnetic methods have been carried out in the area, and a number of exploration boreholes have been completed. However, due to the relative complexity of the geological formations and the relatively small resistivity differences caused by the fracture structures, it is not possible to accurately determine the spreading of the subsurface geological formations based on the results of the existing work.

Based on the actual situation, an area-based survey of the area was carried out using the CSAMT method. From the actual results of the CSAMT, we have inferred the fractures, the stratigraphic distribution and the depth of burial of the granite tops.

Figure 4 illustrates a composite profile obtained from a CSAMT survey in the West Badlands geothermal field. Borehole results have been revealed for hot water in the F2 fracture structure, which was drilled to a depth of less than 300m and produced water at temperatures in excess of 90°C. The resistivity profile results from the acoustic emission geodetic electromagnetic bathymetry inversion show a relatively stable low resistance layer of less than 20  $\Omega$ -m, with a thickness of about 100 m, corresponding to the Quaternary generation; a relatively small resistivity longitudinal gradient with depth variations between  $h = -100-200$  m in the range  $x = 300-800$  m, with a clear horizontal relative low resistance zone, presumably this relative low resistance zone is generated by the Neoproterozoic generation, while the interface of the lower high resistance layer would be the top granite interface. Relatively longitudinal low resistance zones occur around  $x = 650$ m and  $x = 900$ m and these are presumed to have been generated by fracture formations (numbered F2 and F3 respectively), while the relatively low resistance zone between  $x = 500$ m and  $x = 1100$ m, below  $h = -1600$ m, should be the deep thermal reservoir.

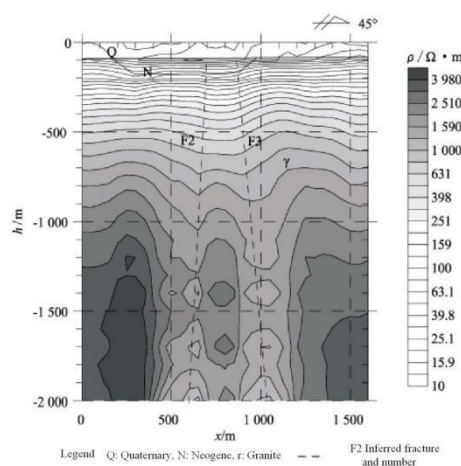


Figure 4 Comprehensive CSAMT survey profile of the West Badlands geothermal field

This is also a typical medium to low temperature convective geothermal field survey result, as the cover layer is very thick and no hot springs are exposed; the shallow thermal storage is located in the fracture tectonic zone, and there is no obvious low resistance zone in the shallow thermal storage. The results of the CSAMT survey clearly

demonstrate the spatial distribution of the thermal storage cover, deep thermal storage and underground hot water channels in the geothermal field, which can provide a reliable basis for further geothermal development.

### VI. ANALYSIS AND INTERPRETATION OF CSAMT DATA

Within the survey area, three mutually parallel CSAMT profiles, K1, K2 and K3, are laid out along the east-west direction. these profiles are almost parallel to the vertical fracture structure. The rock masses in the survey area are relatively homogeneous, with the bedrock and surrounding rocks at depth being mainly granite with high resistance characteristics (see Figure 3). 2D inversions of apparent resistivity and frequency were used to obtain 2D inversion results and interpretations for each line, shown.

The inversion results and geological interpretation of line K1 are shown in Figure 5, which is the focus area for spa exploration in the survey area and is the longest profile at 940 m. The presence of a low resistance zone is evident from the 2D resistivity inversion results, and in particular the profile as a whole can be considered to be of type G stratigraphy. The shallow low-resistance zone is caused by sedimentary infiltration such as human life and precipitation, while the base is a granitic rock mass. Controlled by fractures F and F1, two relatively closed zones of low and medium resistance spatial anomalies exist at depth. Of these, F has a dip of about 80°, while F1 has a dip of roughly 140° [22]. These two fractures form a favorable area of thermal storage at the deep intersection (see Figure 5). Several developed hot springs are located between points 240 and 400 on this survey line, approximately 100m to the north. The correspondence between the x-coordinates of the fracture intersection locations (i.e. favorable thermal storage areas) and the locations of the existing hot springs, as marked in Figure 5, can provide some basis for identifying favorable thermal storage areas on lines K2 and K3.

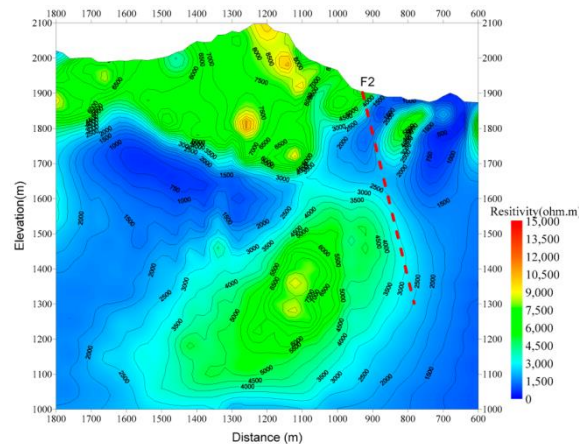


Figure 5 2D inversion resistivity and geological interpretation section of CSAMT method for line K1

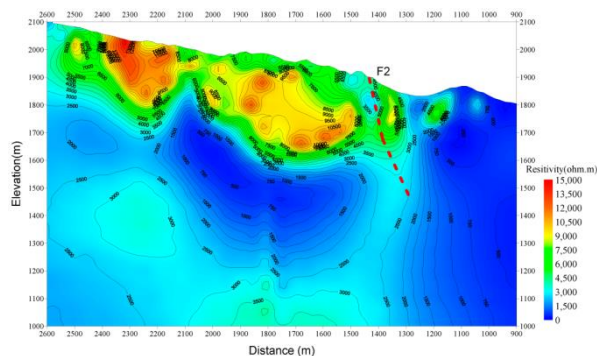


Figure 6 2D inversion resistivity and geological interpretation section of the CSAMT method for line K2

Figure 6 shows the 2D inverse resistivity and geological interpretation cross-section of the CSAMT method for the K2 line. Figure 6(a) shows the resistivity inversion results and Figure 6(b) shows the geological interpretation map inferred from the physical survey. Based on the distribution of resistivity contours, the shallow part of the entire section shows a medium to low resistance feature. Between point 400 and 640, the medium to low resistance feature

extends more downwards and is presumed to consist of weathered Quaternary overburden and weathered granite [23]. The resistivity is essentially below 2000  $\Omega$ -m due to the high water content of the weathered denudation of the ground surface. Based on the distribution characteristics of the resistivity contours and geological data, the location of the main fracture F near point 760 is presumed to extend downwards for about 300m, with the dip of F being about 65°. Near point 320 is presumed to be the location of secondary rupture F1, which has a dip of about 130° and intersects the main rupture F at depth. Near point 480, at an elevation of about 200m, resistivity contours are dense and prominent downwards, with high resistance features beneath them. This area is characterized by the intersection and sharp extinction of the main fracture F with the secondary fracture F1 and is labelled as a favorable thermal storage site at the corresponding location, as shown in Figure 6.

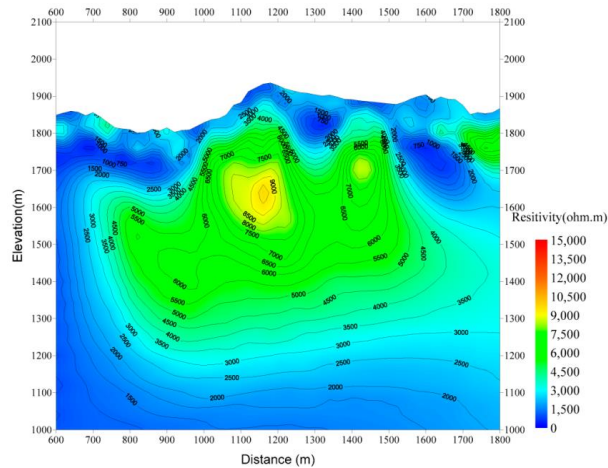


Figure 7 2D inversion resistivity and geological interpretation section of CSAMT method for line K3

Figure 7 illustrates the 2D inverse resistivity and geological interpretation section of the CSAMT method for Line K3. Figure 7(a) shows the resistivity inversion results and Figure 7(b) shows the geological interpretation map inferred from the physical survey. Analysis of the 2D resistivity inversion results shows that the high and low resistance divides are obvious. The resistivity lateral low-resistance stratification appears throughout the profile above 400m above sea level, i.e. the surface shows a low-resistance feature, which is caused by the surface sediment layer generated by the Quaternary or weathered granite at the surface being fully filled with water. Between 100m and 200m above sea level, corresponding to measurement points 80 to 240, there are relatively closed areas of low resistance and the tops of these show dense contours and signs of upward passage. The location of the main fracture F in the survey area is presumed to be in the vicinity of measurement point 180, with a presumed dip of approximately 70° to 80°. The location of the secondary fracture F1 in the survey area is postulated near measurement point 0. This fracture extends from depth to the main fracture F and intersects a low resistance anomaly at depth, with a dip of approximately 120° at F1 [24]. The two fractures are presumed to be flanked by granitic rocks, which provided space for deep water storage due to their dislocation during early geological movement. The fractures extend until they become acutely extinct at about 0m above sea level, and this location is presumed to be a favorable site for thermal storage (Figure 7). The area below 0m to -600m above sea level is clearly characterized by high resistance and is presumed to be a granite body.

The resistivity inversion results and geological interpretation of the three profiles combined indicate that two fracture structures (F and F1) exist in the survey area, which are oppositely inclined and intersect at depth. line K1, line K2 and line K3 show medium to low resistance anomalies at the intersection of the two fractures, with the intersection of lines K1 and K3 being deeper than that of line K2 [25]. The depth of the deep intersection of the two fractures is presumed to be shallower in the middle and deeper on both sides within the measured area. Therefore, it is inferred that the deep low resistance anomalies on the profiles of lines K1 and K3 are more favorable for thermal storage than line K2.

## VII. ANALYSIS OF APPLICATION EFFECTS

### A. Effectiveness of application in the investigation of thermally conductive structures

The effectiveness of the application of the CSAMT method shows that it can help us to find favorable structures for thermal conductivity geothermal. Therefore, the key to the CSAMT method in geothermal investigation work is to find the corresponding structural areas in order to make a judgement based on the characteristics of the structure.

Specifically, we expect formations to have the following characteristics:

The presence of distinct low-resistance closed circles or low-resistance strips in the resistivity profile that are large enough (to qualify for development). These low resistance areas should be clearly visible on the resistivity profile.

A high resistance horizon should be present above the low resistance area and the thickness of this horizon should be reasonable (sufficiently thick). The requirement for a sufficient cover thickness is to effectively protect the thermal resources in the subsurface.

The conditions surrounding the low-resistance area need to be considered in a focused manner. For example, factors such as the presence of discernible thermal conductivity channels or heat sources.

In summary, the CSAMT method allows us to find formations with the above-mentioned characteristics and thus to identify favorable areas for thermal conductivity of the geothermal heat.

### B. Comprehensive Geothermal Exploration Research Results

As a result of the previous analysis, the following summary of the research content of this question is presented:

Firstly, when applying the CSAMT method in highland geothermal, the actual conditions of the site need to be fully considered and combined with the research results of the same industry. For alpine plateau geothermal, we have carried out a zoning process, taking into account a number of factors such as fracture tectonic features, hydrological conditions and depth of thermal storage, and have carried out a systematic zoning process.

Secondly, a geothermal thermal storage tectonic model was developed based on site conditions and used as a tool to compare and analyze geothermal wells in a number of sub-divisions within the region.

The results of the study show that larger scale fracture structures exist around most of the geothermal wells in the region, most of which are located along river valleys. Due to geological movements, river valleys tend to be larger fracture zones, particularly typified by the Xian shui River and Xian shui River fracture zones. Based on the survey results and the geological data of the area, we generated a geothermal conductivity model, which can be seen in Figure 8, after considering all the key information.

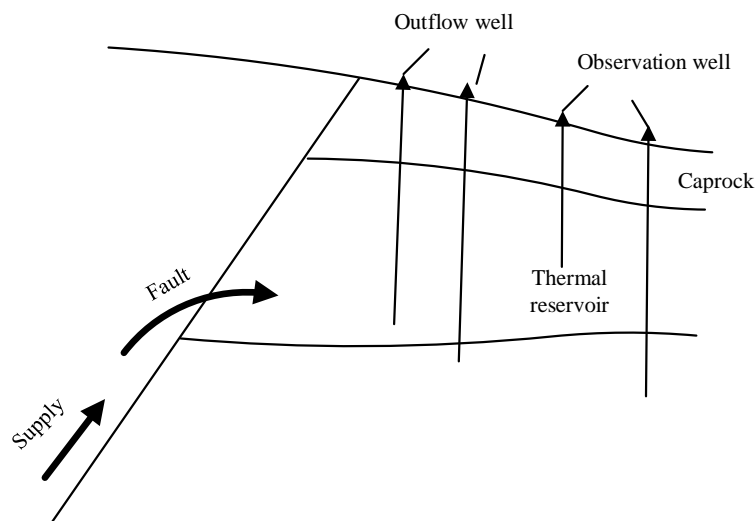


Figure 8 Geothermally induced storage model

## VIII. CONCLUSION

The controlled source audio magnetotelluric method has a sound theoretical foundation and shows strong anti-interference ability and high resolution in engineering applications, which is especially suitable for geothermal exploration around cities. Through example analysis, we have adopted GD-P32II multi-functional electro-magnetic sounding system for field data acquisition, and the results show that the data are stable and reliable, and the exploration effect is remarkable. The method can well reflect the complex fracture tectonic morphology and obviously respond to tectonic units with different electrical properties in the subsurface, providing a reliable basis for identifying favorable thermal storage sites. The CSAMT method has achieved good results in hydrothermal geothermal resource exploration, and can achieve satisfactory exploration results despite human interference around the city. Therefore, in geothermal resources exploration projects, CSAMT method has a broad application prospect.

## ACKNOWLEDGEMENTS

## Funding Statement

This work was supported by. Geological Survey Project of China Geological Survey (DD20230389).

## REFERENCES

- [1] Envelope, B. H. P. , & Guo, J. . (2022). Research on medium - low temperature geothermal power generation system. *Energy Reports*, 8, 553-559.
- [2] Xu, C. , Yu, D. , & Luo, Z. . (2021). Recharge sources and genetic model of geothermal water in tangquan, nanjing, china. *Sustainability*, 13(8), 4449.
- [3] Liu, C. L. , Lu, C. M. , Li, Y. S. , Hao, Q. C. , & Cao, S. W. . (2022). Genetic model and exploration target area of geothermal resources in hongtang area, xiamen, china. *Journal of Groundwater Science and Engineering*, 10(2), 128-137.
- [4] Hendrarsakti, J. , & Rahma, M. . (2021). Numerical study of temperature profiles of transient flow in the geothermal oilfield. *IOP Conference Series: Earth and Environmental Science*, 732(1), 012026 (17pp).
- [5] Envelope, B. H. P. , & Guo, J. . (2022). Experimental study on medium and low temperature geothermal ammonia power generation system based on vertical tube falling film. *Energy Reports*, 8, 723-729.
- [6] Ren, L. W. , Han, Z. P. , Huo, J. W. , & Gao, Y. J. . (2021). Feasibility analysis of low thermal conductivity asphalt concrete bridge deck deicing by using geothermal energy. *IOP Conference Series: Earth and Environmental Science*, 861(3), 032090 (12pp).
- [7] Liu, J. , Zhu, Y. , Miao, Z. , Cui, L. , & Li, D. . (2021). Study on the pretreatment process and removal rules of sulfur-containing compounds for medium- and low-temperature coal tar. *ACS Omega*, 6(19), 12541-12550.
- [8] Guo, Y. , Luo, L. , Zheng, Y. , Wang, J. , & Zhu, T. . (2021). Low-medium temperature application of selective catalytic reduction denitration in cement flue gas through a pilot plant. *Chemosphere*, 276, 130182.
- [9] Luo, Q. , Li, J. , Yan, Q. , Li, W. , & Ding, Y. . (2021). Sliding wear of medium-carbon bainitic/martensitic/austenitic steel treated by short-term low-temperature austempering. *Wear*, 476, 203732.
- [10] Zhang, T. C. . (2021). Innovative arrangements of multiple organic rankine cycles to effectively generate power from the medium-to-low grade of heat source. *Applied thermal engineering: Design, processes, equipment, economics*, 193(1).
- [11] Men, Y. , Liu, X. , & Zhang, T. . (2021). A review of boiler waste heat recovery technologies in the medium-low temperature range. *Energy*, 237, 121560.

- [12] Sogbesan, O. , Garner, C. P. , & Davy, M. H. . (2021). The effects of increasing fame biodiesel content on combustion characteristics and hc emissions in high-egr low temperature combustion. *Fuel*, 302(2), 121055.
- [13] Yudo, H. , & Jokosisworo, S. . (2021). The effect of low tempering, medium tempering, and high tempering heating temperature variations in the type of medium carbon steel st 60 on microstructure, hardness, and toughness. *IOP Conference Series: Materials Science and Engineering*, 1052(1), 012047 (12pp).
- [14] Ceglia, F. , Macaluso, A. , Marrasso, E. , Sasso, M. , & Vanoli, L. . (2020). Modelling of polymeric shell and tube heat exchangers for low-medium temperature geothermal applications. *Energies*, 13(11), 2737.
- [15] Moloney, F. , Almatrafi, E. , & Goswami, D. Y. . (2020). Working fluid parametric analysis for recuperative supercritical organic rankine cycles for medium geothermal reservoir temperatures. *Renewable Energy*, 147, 2874-2881.
- [16] Wang, Y. , Liu, Y. G. , Bian, K. , Zhang, H. L. , Qin, S. J. , & Wang, X. J. . (2020). Seepage-heat transfer coupling process of low temperature return water injected into geothermal reservoir in carbonate rocks in xian county, china. *Journal of Groundwater Science and Engineering*, 8(4), 305-314.
- [17] Luo, C. , Zhao, J. , Wang, Y. , Yin, H. , & Gong, Y. . (2019). Design and experimental research on the combined flash-binary geothermal power generation system driven by low-medium temperature geothermal system. *Thermal Science*, 24, 13-13.
- [18] Ahmad, S. , Farooq, M. , Anjum, A. , & Mir, N. A. . (2019). Squeezing flow of convectively heated fluid in porous medium with binary chemical reaction and activation energy:. *Advances in Mechanical Engineering*, 11(10), 86-99.
- [19] Zhao, N. , Liu, D. , Du, H. , Wang, C. , & Shi, N. . (2019). Investigation on component separation and structure characterization of medium-low temperature coal tar. *Applied Sciences*, 9(20), 4335.
- [20] Mohammadi, K. , & Mcgowan, J. G. . (2019). A thermo-economic analysis of a combined cooling system for air conditioning and low to medium temperature refrigeration. *Journal of Cleaner Production*, 206(P1-1156), 580-597.
- [21] Kong, L. , Dong, K. , Chen, S. , Xia, C. , & Pei, L. . (2019). Aging properties of nitrile rubber in medium under high-low cyclic temperature environment. *IOP Conference Series: Materials Science and Engineering*, 677(2), 022071 (9pp).
- [22] Carrier, A. , Fischanger, F. , Gance, J. , Cocchiararo, G. , & Lupi, M. . (2019). Deep electrical resistivity tomography for the prospection of low-to medium-enthalpy geothermal resources. *Geophysical Journal International*, 219(3), 2056-2072.
- [23] Wang, C. , Li, R. , Liu, C. , & Wang, X. A. . (2019). Effects of medium-low temperature hydrothermal treatment on microstructure and dimensional stability of chinese sweetgum wood. *Wood Research*(1), 64.
- [24] Xiao, X. , Fang, P. , Huang, J. , Wu, H. , Tang, Z. , & Cen, C. . (2019). Pilot scale study on medium/low temperature scr denitration technology for industrial flue gas. *IOP Conference Series: Earth and Environmental Science*, 267(2), 022035 (5pp).
- [25] Nyamsi, S. N. , Tolj, I. , & Lototskyy, M. . (2019). Metal hydride beds-phase change materials: dual mode thermal energy storage for medium-high temperature industrial waste heat recovery. *Energies*, 12(20), 3949.